

A Mucin-Deficient Ocular Surface Mimetic Platform for Interrogating Drug Effects on Biolubrication, Antiadhesion Properties, and Barrier Functionality

Amy C. Madl,¹ Chunzi Liu,¹ Daniel Cirera-Salinas, Gerald G. Fuller, and David Myung*



Cite This: *ACS Appl. Mater. Interfaces* 2022, 14, 18016–18030



Read Online

ACCESS |



Metrics & More



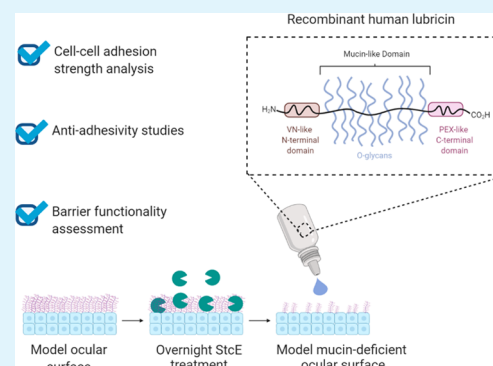
Article Recommendations



Supporting Information

ABSTRACT: Dry eye disease (DED) affects more than 100 million people worldwide, causing significant patient discomfort and imposing a multi-billion-dollar burden on global health care systems. In DED patients, the natural biolubrication process that facilitates pain-free blinking goes awry due to an imbalance of lipids, aqueous medium, and mucins in the tear film, resulting in ocular surface damage. Identifying strategies to reduce adhesion and shear stresses between the ocular surface and the conjunctival cells lining the inside of the eyelid during blink cycles is a promising approach to improve the signs and symptoms of DED. However, current preclinical models for screening ocular lubricants rely on scarce, heterogeneous tissue samples or model substrates that do not capture the complex biochemical and biophysical cues present at the ocular surface. To recapitulate the hierarchical architecture and phenotype of the ocular interface for preclinical drug screening, we developed an *in vitro* mucin-deficient DED model platform that mimics the complexity of the ocular interface and investigated its utility in biolubrication, antiadhesion, and barrier protection studies using recombinant human lubricin, a promising investigational therapy for DED. The biomimetic platform recapitulated the pathological changes in biolubrication, adhesion, and barrier functionality often observed in mucin-deficient DED patients and demonstrated that recombinant human lubricin can reverse the damage induced by mucin loss in a dose- and conformation-dependent manner. Taken together, these results highlight the potential of the platform—and recombinant human lubricin—in advancing the standard of care for mucin-deficient DED patients.

KEYWORDS: lubricin, adhesion, ocular surface, dry eye disease, mucin deficiency



I. INTRODUCTION

The ocular surface is covered by a tear film composed of mucins, water, and lipids, which protect and lubricate the underlying corneal and conjunctival epithelium.^{1–4} Disruptions in tear film homeostasis can result in dry eye disease (DED), a multifactorial ocular pathology afflicting hundreds of millions worldwide.^{5–8} In many DED patients, reduced biosynthesis or loss of functional mucins leads to altered mechanical interactions that drive disease pathophysiology.¹ While these large, hydrophilic, and highly glycosylated extracellular glycoproteins ordinarily maintain wet surfaces, act as a barrier against pathogens, and prevent epithelial–epithelial adhesion during blink cycles,^{2,3,9,10} the mucin-aqueous layer of the tear film is commonly damaged in DED patients, increasing shear stress during spontaneous, physiological blinks and inducing inflammation and patient discomfort.^{1,6,11}

Despite the substantial economic and quality of life burdens imposed by DED,¹² few efficacious therapies are available.^{8,13} In fact, among 26 trials testing 13 potential DED drugs between January 1997 and October 2017, no large ($N > 100$) multicenter studies demonstrated statistical significance for both a primary sign and symptom endpoint.⁸ However, one

investigational therapy—recombinant human lubricin—yielded significant improvements in signs and symptoms of DED without treatment-related adverse effects in a small, randomized clinical trial,¹⁴ spurring interest in lubricin and other biolubricants as potential treatments for DED.¹³

Despite ocular lubricants' promise as DED therapies, their translation from bench to bedside is hindered by a lack of scalable preclinical screening platforms that mimic the complex, hierarchical architecture and morphology of the cornea–palpebral conjunctiva and bulbar conjunctiva–palpebral conjunctiva ocular interfaces. Illustratively, model substrates with hydrophobic or hydrophilic surface properties are commonly employed to interrogate the antiadhesion and lubrication properties of prospective biolubricants.^{15–21}

Received: November 16, 2021

Accepted: March 3, 2022

Published: April 13, 2022



Although these simplified systems are cost-effective and high-throughput, they present nonphysiological surface chemistries that may promote nonrepresentative substrate interactions and self-assembly behavior,¹⁹ reducing their predictive power and potential for mechanistic insight. To partially overcome this limitation, some groups have mimicked the ocular interface by mounting human corneal tissues and either human eyelid tissues or poly(dimethylsiloxane) (PDMS) on mechanical testing machines and articulating the two surfaces against each other in the presence of drug candidates.^{22,23} While tissue isolates better emulate the complex structure of the ocular interface, human samples are scarce and costly, and the surface properties of both the cornea and the eyelid may be compromised during collection, transportation, and storage.²⁴ As membrane-associated mucins affect the physicochemical properties of the ocular surface,²⁵ which in turn affect lubrication behavior,¹⁹ inherent and accidentally induced tissue heterogeneity may bias friction measurements and limit their replicability and comparability.

Immortalized human conjunctival and corneal epithelial cell lines capable of reproducibly differentiating into physiological, stratified cellular layers that retain the mucin expression patterns of native tissues represent a promising alternative to human tissues for high-throughput drug screening studies.^{26–28} We previously reported the development of an *in vitro* mucin-deficient DED model employing these cell lines in a live cell rheometer (LCR) setup to mimic complex ocular interface interactions.²⁹ The mucin-deficient mimetic ocular surface (Mu-DeMOS) model recapitulates the frictional damage observed in mucin-deficient DED patients. Here, we demonstrate the model's potential for biopharmaceutical applications such as preclinical drug screening and quality control by investigating the dose- and conformation-dependent biolubrication properties of recombinant human lubricin, a promising investigational therapy for DED, on model ocular interfaces. Furthermore, we exploit the compatibility of the dry eye mimetic ocular surfaces with imaging-based techniques to model and interrogate a range of clinically relevant drug–tissue interactions, including adsorption, barrier protection, and antiadhesion properties. Together, the results indicate that recombinant human lubricin may ameliorate pathological changes observed at mucin-deficient ocular surfaces and highlight the utility of the Mu-DeMOS-based platform as an ophthalmologic drug screening tool.

II. RESULTS AND DISCUSSION

II.I. Immortalized Human Corneal and Conjunctival Epithelial Cells Mimic Physiological Properties of Native Ocular Tissues. The native ocular surface comprises two epithelia: the central corneal epithelium and the surrounding conjunctival epithelium, each of which exists as a nonkeratinized, stratified structure.³⁰ The conjunctiva extends from the inside of the eyelid to the periphery of the cornea, forming a thin, mucin-rich lining over the white of the eye (bulbar conjunctiva) and the posterior eyelid surface (palpebral conjunctiva). Both hTERT-immortalized human conjunctival epithelial cell (HCjE)²⁶ and hTERT-immortalized human corneal epithelial cell (hTCEpi)²⁷ monolayers have previously been shown to differentiate, stratify, and express membrane-associated mucins when cultured in high-calcium, serum-containing medium, mimicking the physiological properties of the native conjunctival and corneal epithelia.^{25–27}

The LCR was designed and custom-built to enable quantitative measurements of the average mechanical properties of entire cellular monolayers with adherent geometry and native cell–cell and cell–substrate contacts.^{29,31–33} LCRs have previously been harnessed to quantify stromal vascular cell mechanics,³¹ examine corneal cell adhesion to contact lens materials,³² and investigate curli-mediated adhesion of uropathogenic *Escherichia coli* to bladder epithelial cells.³³ In the Mu-DeMOS model, HCjE or hTCEpi cells are cultured on customized, collagen-coated 35 mm cell imaging dishes with a glass bottom to recapitulate the conjunctival or corneal epithelium, respectively.²⁹ Over the course of 7 days in stratification medium containing the DMEM/F12 medium with high calcium (1 mM CaCl₂), 10% fetal bovine serum, and 10 ng/mL EGF, both cell lines differentiate, stratify, and adopt elongated phenotypes (Figure S1A,B). Additionally, both cell lines express membrane-associated mucins at their apical surfaces, including MUC1, a monomeric mucin expressed at the native ocular surface by both corneal and conjunctival epithelial cells,^{1,9,34} as evidenced by general O-glycan labeling with Jacalin and MUC1 immunocytochemistry. However, HCjE cells demonstrated less uniform apical mucin layers, with some subapical mucin expression observed (Figure S1B). Notably, native corneal epithelial cells typically only express membrane-associated mucins such as MUC1 at their apical cell membranes, while native conjunctival epithelial cells are known to express membrane-associated mucins apically and subapically.²

II.II. StcE, a Mucin-Specific Protease, Induces Mucin Deficiency and Frictional Damage at Mimetic Ocular Interfaces, Effects Reversed by Recombinant Human Lubricin Supplementation. Mucins play a critical role in maintaining the integrity of the ocular surface. In the healthy eye, MUC1 and other membrane-bound mucins form a glycocalyx about 200–500 nm thick at the surface of corneal and conjunctival epithelial cells and exhibit antiadhesive properties.^{2,3,35} These mucins reduce abrasive stress during boundary lubrication and prevent adhesion of the corneal epithelium and the palpebral conjunctiva lining the eyelid during blinking and sleeping.⁹ Additionally, negatively charged, hydrophilic membrane-associated mucins alter the surface properties of the corneal and conjunctival epithelia.^{7,29}

To recapitulate the mucin deficiency that leads to altered surface chemistry and mechanical interactions in DED, live, stratified HCjE and hTCEpi cells in the Mu-DeMOS model are treated with recombinant StcE, a mucin-specific protease.^{29,36–38} StcE is a zinc metalloprotease secreted by enterohemorrhagic *E. coli* to remodel the mucosal lining of the gastrointestinal tract during infection.³⁷ The enzyme specifically recognizes α -O-glycan-containing substrates with a peptide consensus sequence of S/T^{*}-X-S/T, where X is any amino acid.^{36,37} This peptide consensus sequence is common within the mucin family, and recombinant StcE has previously been found to be active against human mucins in a dose-dependent manner.³⁶ Moreover, StcE is a robust enzyme that retains its activity from pH 6.1 to 9.0 over a broad range of salt concentrations, as well as in the presence of protease and serum-containing cell culture medium.³⁸

During LCR experiments, a top plate with stratified conjunctival epithelial cells is gently brought into contact with multilayers of conjunctival or corneal epithelial cells cultured on a bottom plate and allowed to settle by gravity (Figure 1A). After at least 2 h of physical contact at

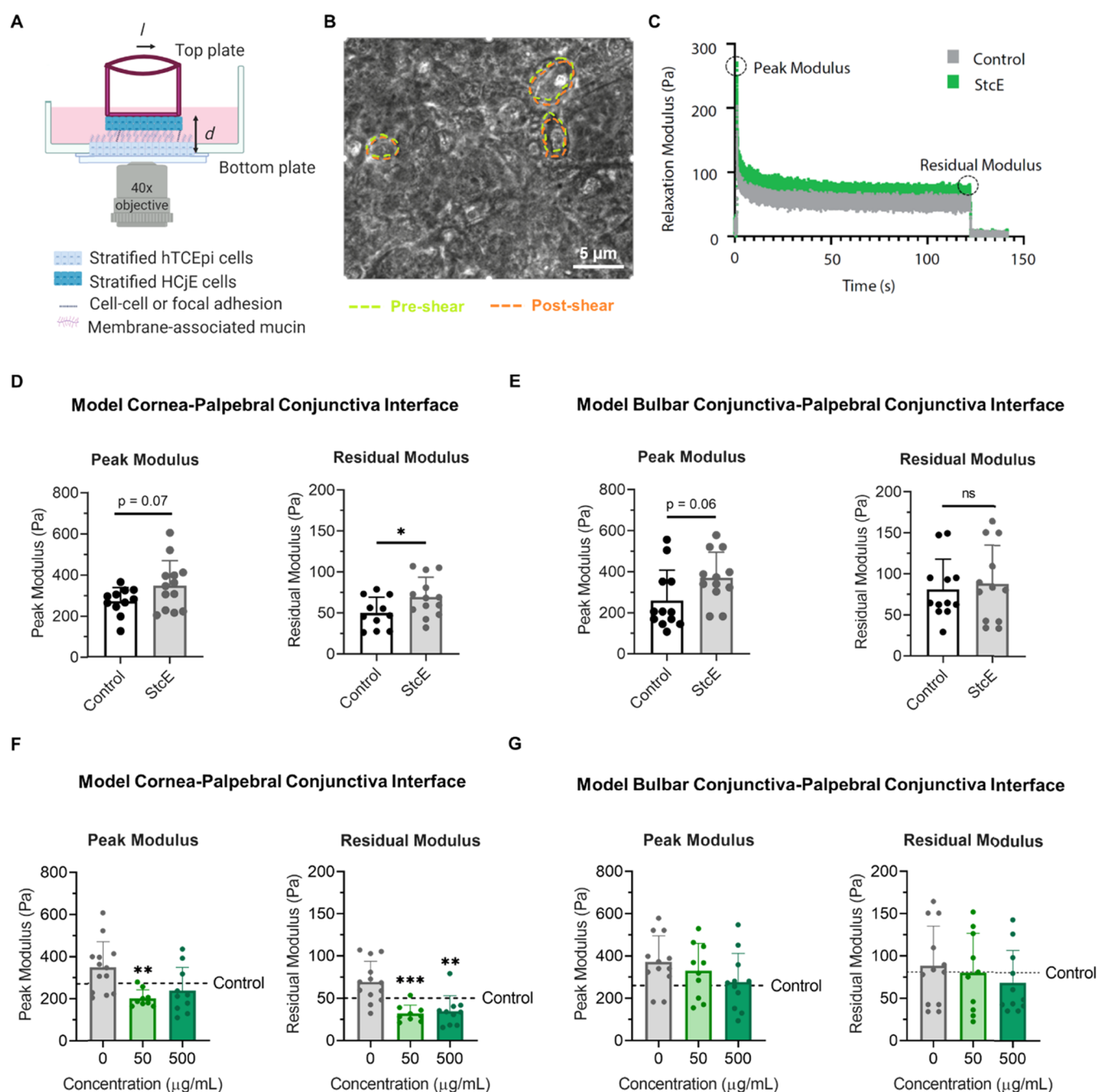


Figure 1. Mucin-specific protease StcE-induced frictional damage at model cornea–palpebral conjunctiva and bulbar conjunctiva–palpebral conjunctiva interfaces. **(A)** Idealized schematic of the LCR setup for the model cornea–palpebral conjunctiva interface immersed in cell culture medium, in which differentiated HCjE cells on the top plate laterally shear differentiated hTCEpi cells on the bottom plate. **(B)** Representative image showing the shearing of hTCEpi cells following a $5\ \mu\text{m}$ displacement of the top plate, with green and orange dashed lines highlighting cell boundaries before displacement (not otherwise shown) and after displacement, respectively. **(C)** Representative LCR stress relaxation curve for the model cornea–palpebral conjunctiva interface with and without StcE treatment. **(D, E)** Peak and residual moduli for LCR experiments shearing **(D)** control and StcE-treated differentiated HCjE cells against control and StcE-treated hTCEpi cells (data: mean \pm SD, $n = 11$ (control), 13 (StcE)) or **(E)** control and StcE-treated differentiated HCjE cells against control and StcE-treated differentiated HCjE cells (data: mean \pm SE, $n = 12$). Statistical significance ($p < 0.05$) was determined using two-tailed Welch's t -tests. **(F, G)** Lubricin supplementation attenuated the increase in peak and residual moduli observed when the differentiated cell layers were StcE treated at the **(F)** model cornea–palpebral conjunctiva but not at the **(G)** model bulbar conjunctiva–palpebral conjunctiva interface (data = mean \pm SD, $n = 9$ –13). Statistical significance ($p < 0.05$) was determined using one-way Welch's ANOVA with post-hoc Dunnett's T3 multiple comparisons testing relative to StcE-treated ($0\ \mu\text{g}/\text{mL}$) cells.

physiological temperature to enable focal and cell–cell adhesion formation between the stratified cell layers, the top plate is rapidly translated $5\ \mu\text{m}$ horizontally by the movement of a piezoelectric stage connected to a force transducer, which maintains contact with the top plate's custom stand and

collects stress information at ambient temperature (Figure 1B,C). The movement of the top plate laterally shears the stratified conjunctival epithelial cells against the cells cultured on the bottom plate with low surface pressure ($18.7 \pm 1.8\ \text{Pa}$) (Figure 1B), as the normal force is solely attributable to the

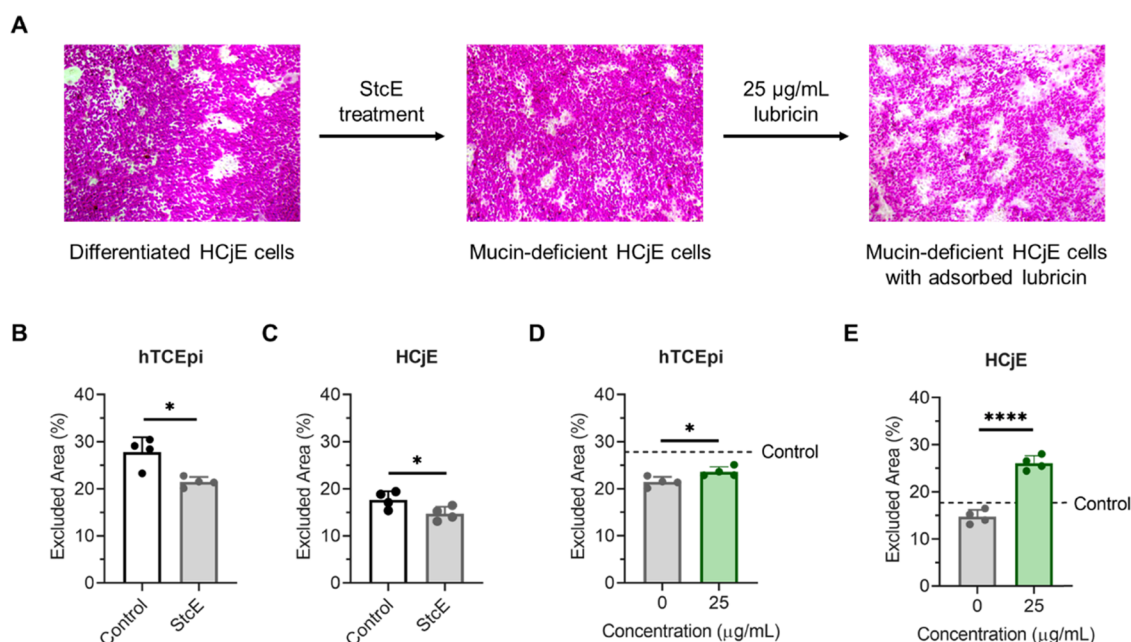


Figure 2. Induced mucin deficiency increased rose bengal penetration for differentiated hTCEpi and HCjE cells, an effect attenuated by lubricin addition. (A) Rose bengal staining in differentiated HCjE cells. Islands of rose bengal-negative cells appeared after 7 days in stratification medium. StcE-induced mucin deficiency increased dye penetration, which was reversed following 2 h supplementation with 25 µg/mL recombinant human lubricin. (B, C) Effect of overnight StcE treatment on rose bengal uptake for (B) hTCEpi and (C) HCjE cells. (D, E) Effect of 25 µg/mL lubricin supplementation on rose bengal uptake in StcE-treated (0 µg/mL) hTCEpi (D) and HCjE (E) cells. Statistical significance ($p < 0.05$) was determined using a two-tailed Welch's *t*-test.

low mass of the coverslip and custom top plate mount.³² The step strain, estimated at $\gamma = 0.173$ and 0.185 for hTCEpi-on-HCjE and HCjE-on-HCjE, respectively, imparts greater stress if there is adhesion between the two cell layers, which is partially relieved as fragile adhesions are broken and structural rearrangements occur within the stratified cell layers. As the LCR is housed within a microscope, cell attachment can be visually monitored during the step strain.

To provide a quantitative measure of adhesion, force recordings are used to calculate a zero-time relaxation modulus (peak modulus) and a long-time relaxation modulus (residual modulus). The apparent relaxation modulus of the cellular layers is calculated as $G_{r,app} = \sigma/\gamma$, where the stress σ is calculated from the force F recorded by the force transducer and the top plate coverslip area A , which is assumed to be the contact area between the stratified cells on the top and bottom plates, as $\sigma = F/A$. The true contact area may be less than the top plate coverslip area A due to surface roughness. The strain γ undergone during the step strain is estimated as $\gamma = l/d$, where l is the stage displacement and d is the gap distance between the basal surface of the bottom plate cells and the basal surface of the top plate cells. Gap distance d was assumed to be constant because StcE treatment and StcE treatment followed by supplementation with 250 µg/mL recombinant human lubricin did not significantly affect the gap distance for Hoechst-labeled differentiated HCjE cells in contact with Hoechst-labeled differentiated hTCEpi or HCjE cells (Figure S2B–E).

Notably, the apparent relaxation modulus is a complex superposition of restoring forces of the cell bodies and the number and strength of adherent contacts; it does not correspond to a classical relaxation modulus.^{29,39} Additionally, while the initial displacement of the top plate mimics the first phase of a blink cycle, the displacement is maintained to

quantitatively measure adhesive strength at the cell–cell interface. Specifically, the cell–cell interface subject to the step-strain deformation exhibits a relaxation behavior with an initial peak modulus that reflects the short time behavior of the cellular layers in response to mechanical perturbation. During this short time behavior, the cytoskeletons of the cells are effectively frozen and interfacial adhesions remain intact. As the displacement is maintained, the modulus decreases to a stable, non-zero plateau value through the breakage of weak intermolecular interactions and rearrangement of cellular components toward a minimal energy conformation with stable interfacial adhesions. Accordingly, the residual modulus correlates with adhesive strength at the cell–cell interface.

In the Mu-DeMOS LCR model, mucin deficiency increases friction between differentiated conjunctival epithelial cells and either stratified conjunctival or corneal epithelial cells without altering cellular mechanics, mimicking the frictional damage observed at the mucin-deficient DED palpebral conjunctiva–bulbar conjunctiva and palpebral conjunctiva–cornea interfaces (Figures 1A–E and S2A–E). Consistent with previous reports that recombinant human lubricin may serve as an effective topical treatment for DED,¹⁴ the addition of either 25 or 250 µg/mL lubricin reduced the observed relaxation moduli, indicating a partial reversal of the pathological phenotype (Figure 1F,G).

While the effects of mucin deficiency on hTCEpi surface roughness and adhesive strength at hTCEpi-on-HCjE cellular interfaces have previously been reported,²⁹ other important properties for biolubricant screening, such as barrier functionality and static antiadhesiveness, remain underexplored. Here, the organic anionic dye rose bengal was used to assess whether induced mucin deficiency reduces the barrier functionality of differentiated corneal and conjunctival epithelial cells. Rose bengal is commonly employed in clinical

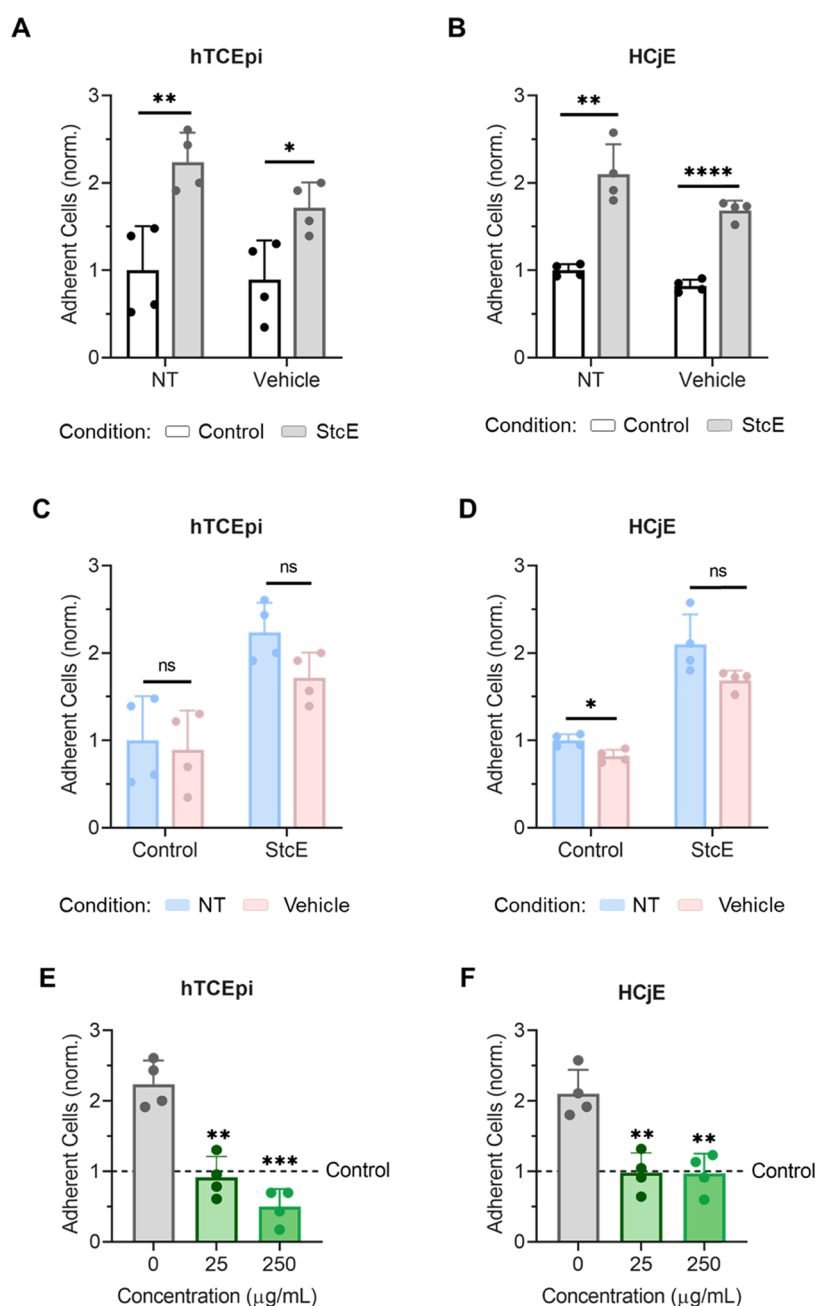


Figure 3. Induced mucin deficiency reduced the antiadhesive character of differentiated hTCEpi and HCjE cells, an effect attenuated by lubricin addition. (A, B) CellTracker Deep Red-labeled HCjE cells in suspension showed significantly increased binding to differentiated (A) hTCEpi and (B) HCjE cells following StcE treatment in both cell culture medium (NT) and cell culture medium containing vehicle (Vehicle) (data = mean \pm SD, $n = 4$). Statistical significance ($p < 0.05$) was determined using two-tailed Welch's t -tests. (C, D) Binding of CellTracker Deep Red-labeled HCjE cells in suspension was not significantly affected by the presence of vehicle for control cells or StcE-treated cells (data = mean \pm SD, $n = 4$). Statistical significance ($p < 0.05$) was determined using two-tailed Welch's t -tests. (E, F) Supplementation with recombinant human lubricin restored the antiadhesive character of StcE-treated (E) hTCEpi and (F) HCjE cells (data = mean \pm SD, $n = 4$). Statistical significance ($p < 0.05$) was determined using one-way Welch's ANOVA with post-hoc Dunnett's T3 multiple comparisons testing relative to StcE-treated (0 $\mu\text{g/mL}$) cells.

practice to assess ocular surface damage. In DED patients, rose bengal application results in patchy ocular surface staining, with dye uptake believed to occur in MUC16-deficient areas.^{40–42} For both differentiated hTCEpi and HCjE cells, overnight treatment with 0.5 $\mu\text{g/mL}$ StcE increased rose bengal penetration, consistent with the pathological phenotype (Figure 2A–C). Media supplementation with the mucin-like glycoprotein lubricin for 2 h prior to staining attenuated dye uptake, suggesting that damage to the protective mucin layer

may be reversible for both corneal epithelial and conjunctival cells (Figure 2D,E).

To further confirm that StcE-induced mucin deficiency broadly recapitulates the DED phenotype and enables robust biolubricant screening, the antiadhesive character of differentiated hTCEpi and HCjE cells was probed. Cell surface-associated mucin O -glycans impart antiadhesive character to the apical surface of stratified corneal epithelial cells,³⁵ which is dysregulated in patients with DED. In these experiments, undifferentiated HCjE cells in suspension were labeled with

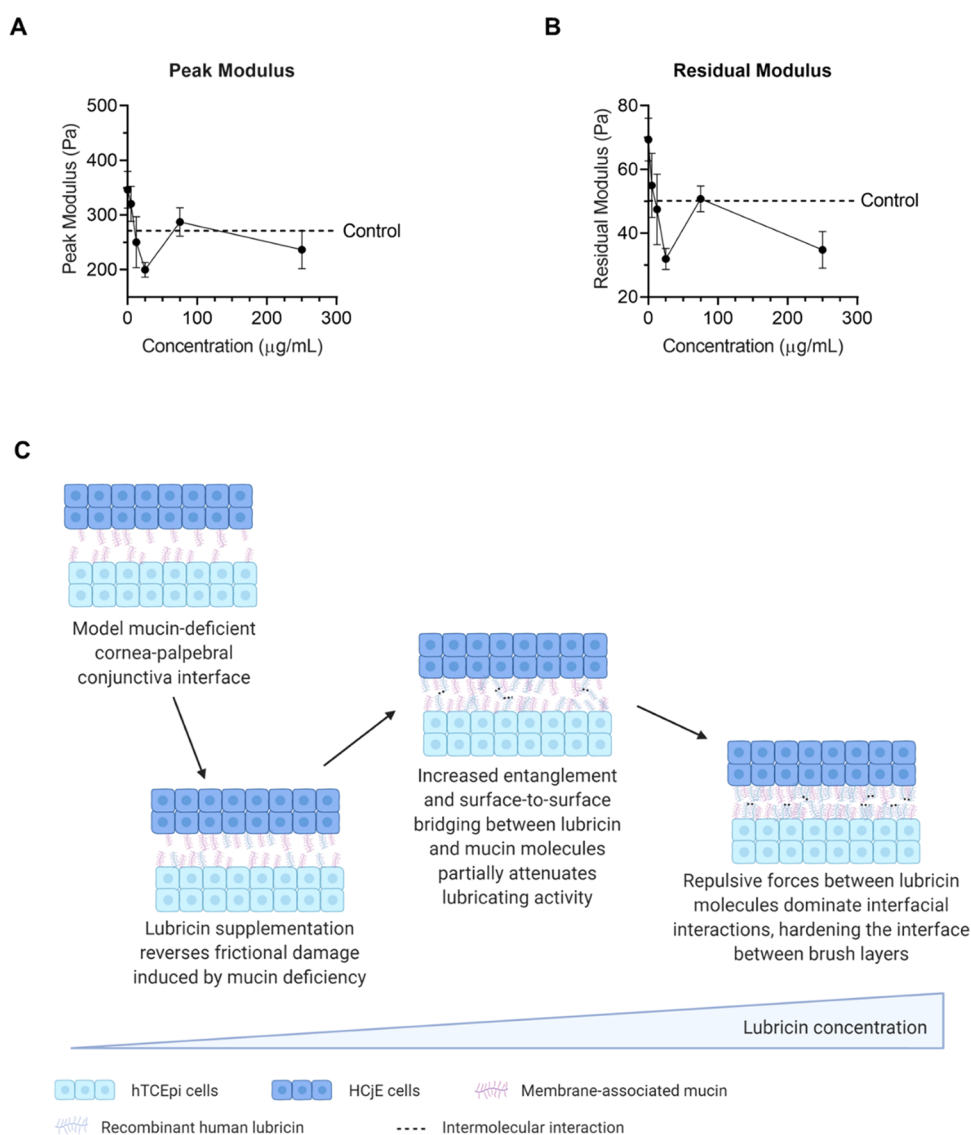


Figure 4. Recombinant human lubricin exhibited dose-dependent biolubrication properties at model mucin-deficient cornea–palpebral conjunctiva interfaces. (A) Peak modulus exhibited a concentration-dependent response ($p < 0.0029$) to lubricin supplementation (data = mean \pm SE, $n = 7–13$). (B) Lubricin supplementation also reduced the residual modulus in a dose-dependent manner ($p < 0.0011$) (data = mean \pm SE, $n = 7–13$). (C) Idealized schematic showing possible mechanism behind observed dose-dependent biolubrication effects at dry eye mimetic ocular surfaces. Statistical significance ($p < 0.05$) was determined using one-way Welch's ANOVA (A, B).

CellTracker Deep Red and allowed to adhere to control and StcE-treated differentiated cell surfaces for 1 h in static culture. Consistent with the antiadhesive properties of membrane-associated mucins, the apical surfaces of control cell layers were significantly more antiadhesive than StcE-treated hTCEpi and HCjE cells in cell culture medium with and without formulation buffer (Figure 3A–D). Moreover, as with rose bengal penetrance, lubricin supplementation attenuated the pathological phenotype observed for StcE-treated hTCEpi and HCjE cells (Figure 3E,F), further indicating that mucin-related ocular surface damage can be reversed.

II.III. Recombinant Human Lubricin Exhibits Non-monotonic Dose-Dependent Biolubrication Properties on Dry Eye Mimetic Ocular Surfaces. Phase I clinical trials for recombinant human lubricin employed 150 $\mu\text{g}/\text{mL}$ lubricin to evaluate its safety and efficacy in patients with moderate DED,¹⁴ a concentration comparable to the estimated lubricin content of synovial fluid ($\sim 200 \mu\text{g}/\text{mL}$).⁴³ Intriguingly, 25 $\mu\text{g}/$

mL lubricin performs similarly to a 10-fold higher concentration (250 $\mu\text{g}/\text{mL}$) on Mu-DeMOS surfaces. Prior studies applying low concentrations of lubricin on model surfaces and cartilage tissues suggest that even quantities of lubricin insufficient for achieving full surface coverage may exert antiadhesion properties and reduce shear stresses at interfaces.^{19,44–46} For example, on hydrophobic self-assembled monolayers of methyl-terminated thiols, adding lubricin from the human synovial fluid at a low, submonolayer coverage concentration (25 $\mu\text{g}/\text{mL}$) reduced friction in the boundary lubrication regime; however, as lubricin concentration increased, friction rose from the local minimum in a concentration-dependent manner up to about 200 $\mu\text{g}/\text{mL}$, at which point monolayer coverage was achieved and friction became independent of solution concentration.⁴⁵ By contrast, addition of lubricin between hydrophilic self-assembled monolayers of hydroxyl-terminated thiols increased friction

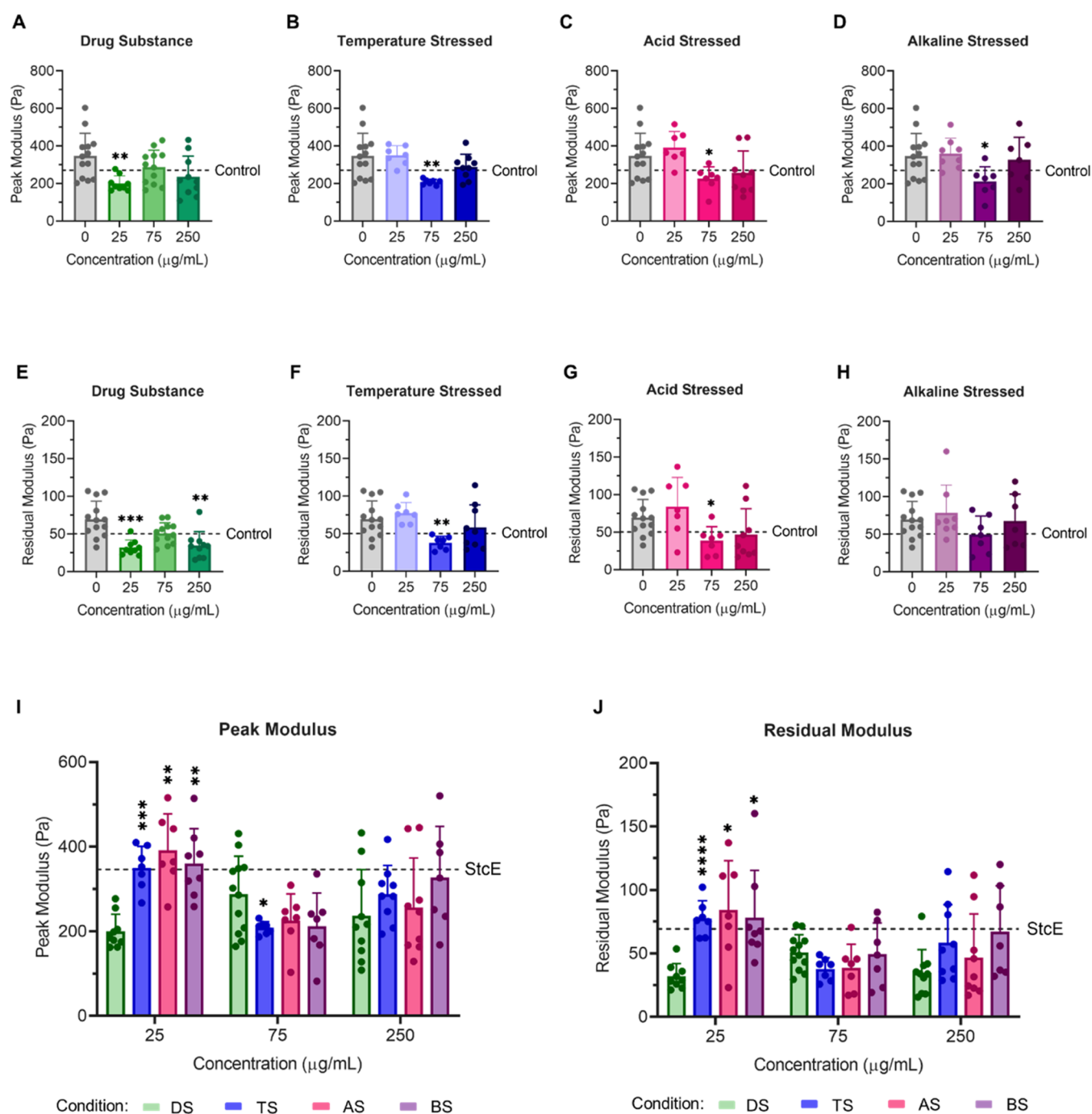


Figure 5. Lubricin molecules subjected to accelerated aging conditions still exhibited dose-dependent biolubrication properties at model cornea–palpebral conjunctiva interfaces. Peak (A–D) and residual (E–H) modulus values for StcE-treated model cornea–palpebral conjunctiva interfaces in the presence of (A, E) unstressed drug substance and (B, F) temperature-stressed, (C, G) acid-stressed, and (D, H) alkaline-stressed lubricin (I, J) at 0, 25, 75, and 250 $\mu\text{g/mL}$. Stressed lubricin molecules exhibited attenuated biolubrication properties at 25 $\mu\text{g/mL}$, with significantly higher (I) peak and (J) residual modulus values observed. Statistical significance ($p < 0.05$) was determined using one-way Welch's ANOVA with post-hoc Dunnett's T3 multiple comparisons testing relative to StcE-treated (0 $\mu\text{g/mL}$) cells (A–H) or unstressed drug substance (DS) (I, J).

until about 200 $\mu\text{g/mL}$, at which point interfacial interactions appeared to be solely between adsorbed lubricin molecules.⁴⁵

As lubricin–substrate interactions are highly specific and influence lubricin adsorption, conformation, and self-assembly, which in turn affect the glycoprotein's lubricating properties,^{19,47,48} the Mu-DeMOS model provides an ideal platform for assessing concentration-dependent effects in the eye, where lubricin interactions are understudied. In contrast to previously presented substrates,^{23,46,49} the dry eye mimetic ocular surfaces

employed in the LCR present live, stratified cells with mucin-deficient apical surfaces and enable physiological focal and cell–cell adhesions to form at the model interface. Because the N- and C-terminal domains of lubricin exhibit significant sequence homology to vitronectin and hemopexin, respectively, and may bind to cellular receptors and cell-secreted extracellular matrix proteins,^{15,16,50,51} presenting physiological surfaces enables more rigorous studies of lubricin interactions at the ocular interface. Moreover, supplementing lubricin in

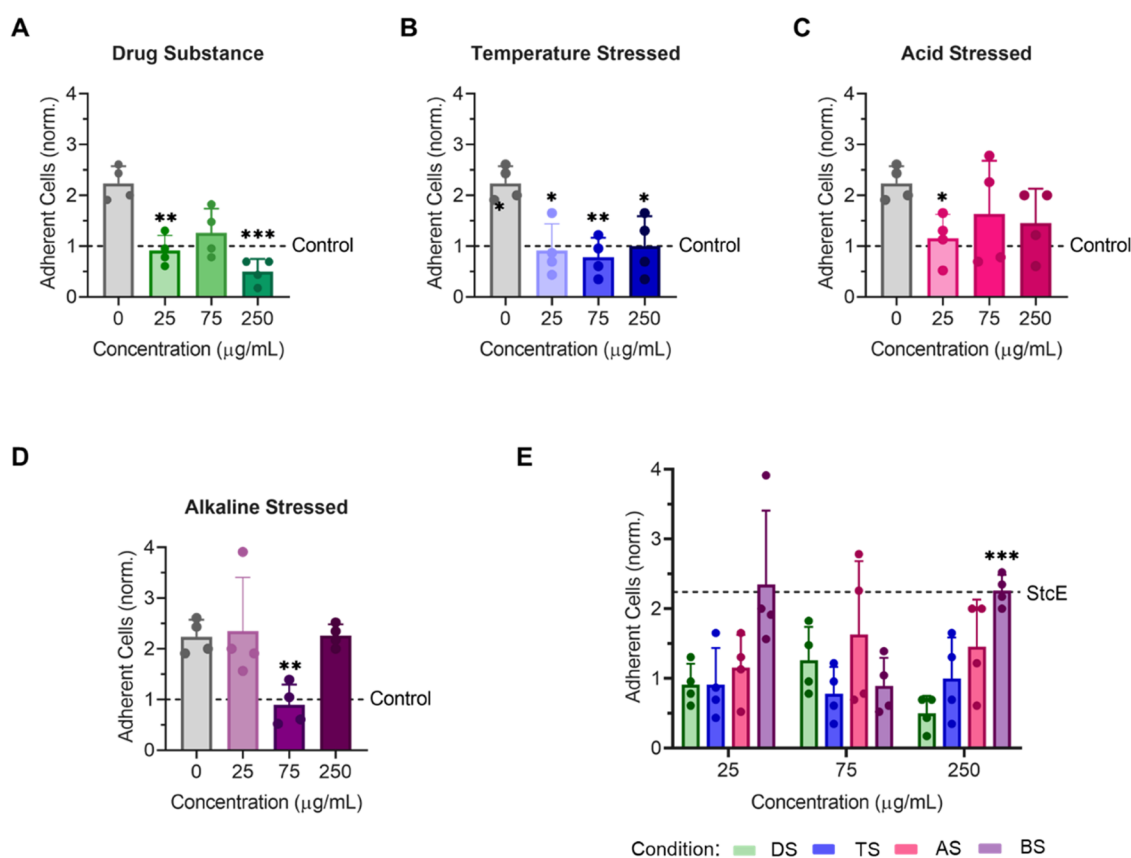


Figure 6. Lubricin subjected to accelerated aging conditions still exhibited antiadhesive properties on StcE-treated differentiated hTCEpi cells. Supplementation with unstressed recombinant human lubricin (A) and lubricin subjected to temperature stress (B), acid stress (C), or alkaline stress (D) reduced the adhesion of CellTracker Deep Red-labeled HCjE cells in suspension to StcE-treated hTCEpi cells (data = mean \pm SD, $n = 4$). (E) Subjecting lubricin to accelerated aging conditions resulted in more variable antiadhesive properties. Statistical significance ($p < 0.05$) was determined using one-way Welch's ANOVA with post-hoc Dunnett's T3 multiple comparisons testing relative to StcE-treated (0 $\mu\text{g/mL}$) cells (A–D) or unstressed drug substance (DS) (E).

cell culture medium, which contains calcium ions and proteins such as albumin that are natively present in the tear film and known to affect lubricin adsorption,^{18,52} enhances the model's predictive power.

To assess the dose dependence of recombinant human lubricin on dry eye mimetic ocular surfaces, 5, 12.5, 25, 75, or 250 $\mu\text{g/mL}$ lubricin was incorporated into the cell culture medium prior to contacting the top plates with HCjE cells and bottom plates with hTCEpi cells (Figure 4A,B). Notably, increasing lubricin concentration between 5 and 25 $\mu\text{g/mL}$ reduced both the peak and residual modulus in a dose-dependent manner, indicating the number or strength of adhesions at the model cornea–eyelid interface decreased as more lubricin was added. However, increasing lubricin concentration from 25 to 75 $\mu\text{g/mL}$ resulted in a statistically significant rise in both the peak and residual modulus values ($p = 0.0087$ and 0.0019 , respectively, in two-tailed Welch's t -tests); further lubricin supplementation up to 250 $\mu\text{g/mL}$ appeared to at least partially reverse the increase in frictional damage, with no statistically significant difference in relaxation moduli found between 250 $\mu\text{g/mL}$ and either 25 or 75 $\mu\text{g/mL}$ lubricin. Intriguingly, a similar trend in equilibrium friction coefficients was previously reported for cartilage explants incubated in lubricin-containing solutions under moderate ($\epsilon = 20\%$) normal strain.⁵³

The C-terminal region (exons 7–12) of lubricin is known to bind cartilage tissues.⁵⁴ However, the N-terminal region (exons

2–5) does not efficiently bind to cartilage; instead, this globular, nonglycosylated domain spontaneously dimerizes through interactions between its cysteine-rich domains.⁵⁴ While the N-terminus is not directly involved in substrate binding, higher-order structures and lubricin aggregates resulting from oligomerization of the N-terminal domains may influence lubrication properties—disulfide bond disruption significantly attenuates lubricin adsorption and antiadhesion properties.^{50,54,55} The extended conformation predicted from lubricin fragment studies—in which the C-terminus anchors lubricin on the surface and the N-terminus extends apically to participate in entanglement interactions and intramolecular and intermolecular bridging—resembles the tail-like conformations previously reported for lubricin on hydrophilic model surfaces, where lubricin appears to adsorb primarily along its hydrophilic, mucin-like central domain.^{17,44} Under low loads, it has been speculated that tails may readily align along a shearing direction, reducing friction more substantially than sterically constrained loops in which both terminal domains contact the surface.¹⁷

While LCR experiments do not provide molecular-level insight into lubricin–substrate interactions at complex cellular interfaces, the observed increase in friction at intermediate lubricin concentration may result from additional interactions between lubricin molecules (Figure 4C). Specifically, as adsorbed lubricin concentration increases on the dry eye mimetic ocular surfaces, additional entanglements and surface-

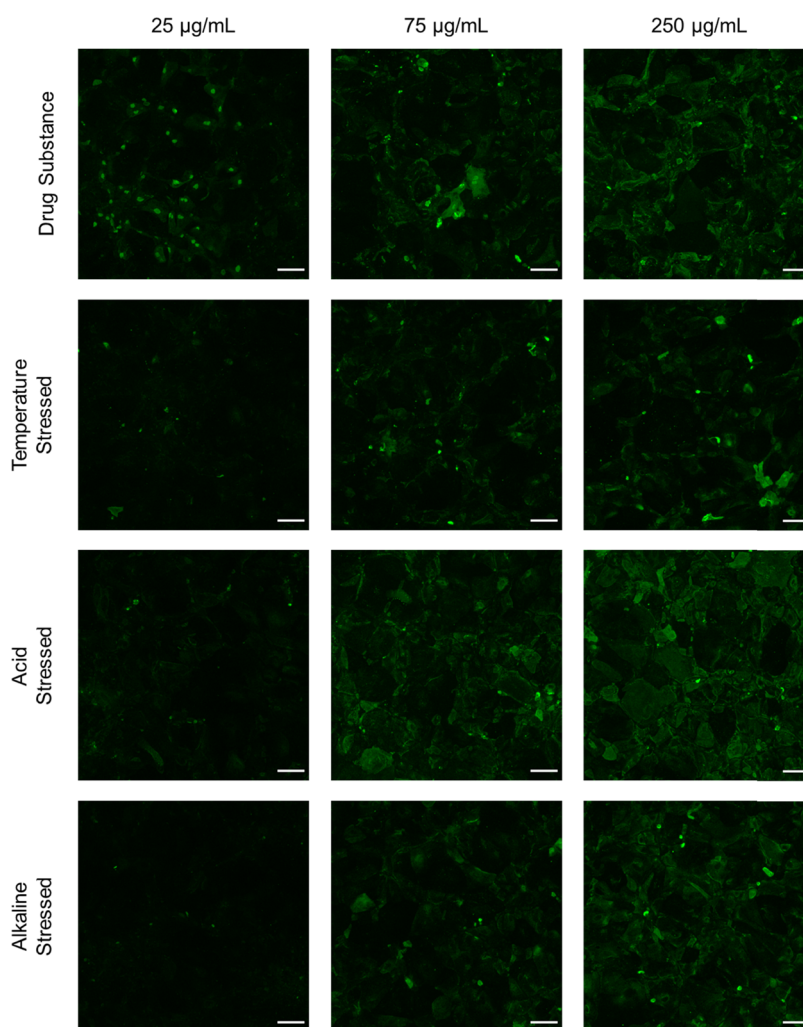


Figure 7. Recombinant human lubricin and lubricin subjected to accelerated aging conditions adsorbed to StcE-treated differentiated hTCEpi cells in a dose-dependent manner (scale bar: 100 μm).

to-surface bridging between lubricin and mucin molecules may partially attenuate lubricin's biolubrication activity. However, as lubricin surface coverage increases further, repulsive forces between lubricin molecules may dominate other interfacial and surface interactions, hardening the interface between brush layers and restoring brush-on-brush lubrication.

II.IV. Accelerated Aging Alters Lubricin Conformation and Lubrication Activity. To interrogate the effects of lubricin conformation on dry eye mimetic ocular surface interactions, recombinant lubricin molecules subjected to three different accelerated aging procedures were employed in LCR experiments at three different concentrations (25, 75, 250 $\mu\text{g}/\text{mL}$) (Figure S3A, Table S1). First, lubricin molecules were incubated for 2 weeks at pH 4.0 and 40 $^{\circ}\text{C}$ (acid stressed (AS)), resulting in significant fragmentation (Figure S3B, Table S1). Second, lubricin molecules were incubated for two weeks at pH 9.0 and 40 $^{\circ}\text{C}$ (alkaline/base stressed (BS)); alkaline stress yielded material with a substantial number of aggregates and some fragmentation (Figure S3B,C, Table S1). Third, lubricin molecules were incubated for 4 weeks at pH 7.0 and 40 $^{\circ}\text{C}$ (temperature stressed (TS)), which also produced a mixture of aggregates and fragments (Figure S3B,C, Table S1). Significantly fewer aggregates were observed following temperature stress at neutral pH compared to alkaline pH (Table S1).

For all three lubricin materials subjected to accelerated aging, the antiadhesion effect of 25 $\mu\text{g}/\text{mL}$ lubricin was attenuated at physiologically relevant pH (Figure 5, Table S2). However, supplementation with 75 $\mu\text{g}/\text{mL}$ aged lubricin significantly reduced friction at the mucin-deficient model cornea–palpebral conjunctiva interface for all stressed variants (Figure 5B–D,F–H). Notably, the aggregated temperature-stressed and alkaline-stressed lubricin molecules exhibited modest intermediate concentration activity attenuation between 75 and 250 $\mu\text{g}/\text{mL}$, similar to the activity reduction observed between 25 and 75 $\mu\text{g}/\text{mL}$ for unstressed lubricin drug substances. Intriguingly, no intermediate concentration behavior was observed for fragmented acid-stressed lubricin molecules, which lack at least one cysteine-rich terminal domain and are thus less likely to engage in surface-to-surface bridging interactions. Similarly, the dose-dependent antiadhesion properties of temperature-stressed and alkaline-stressed lubricin followed a similar trend to unstressed drug substance, albeit at higher concentrations (Figure 6). Unstressed and stressed lubricin molecules exert weakly correlated antiadhesion and biolubrication activity, although the correlation improves when acid-stressed lubricin is excluded from the analysis (peak modulus: Spearman $r = 0.68$, $p = 0.05$; residual modulus: Spearman $r = 0.73$, $p = 0.03$) (Figure S4).

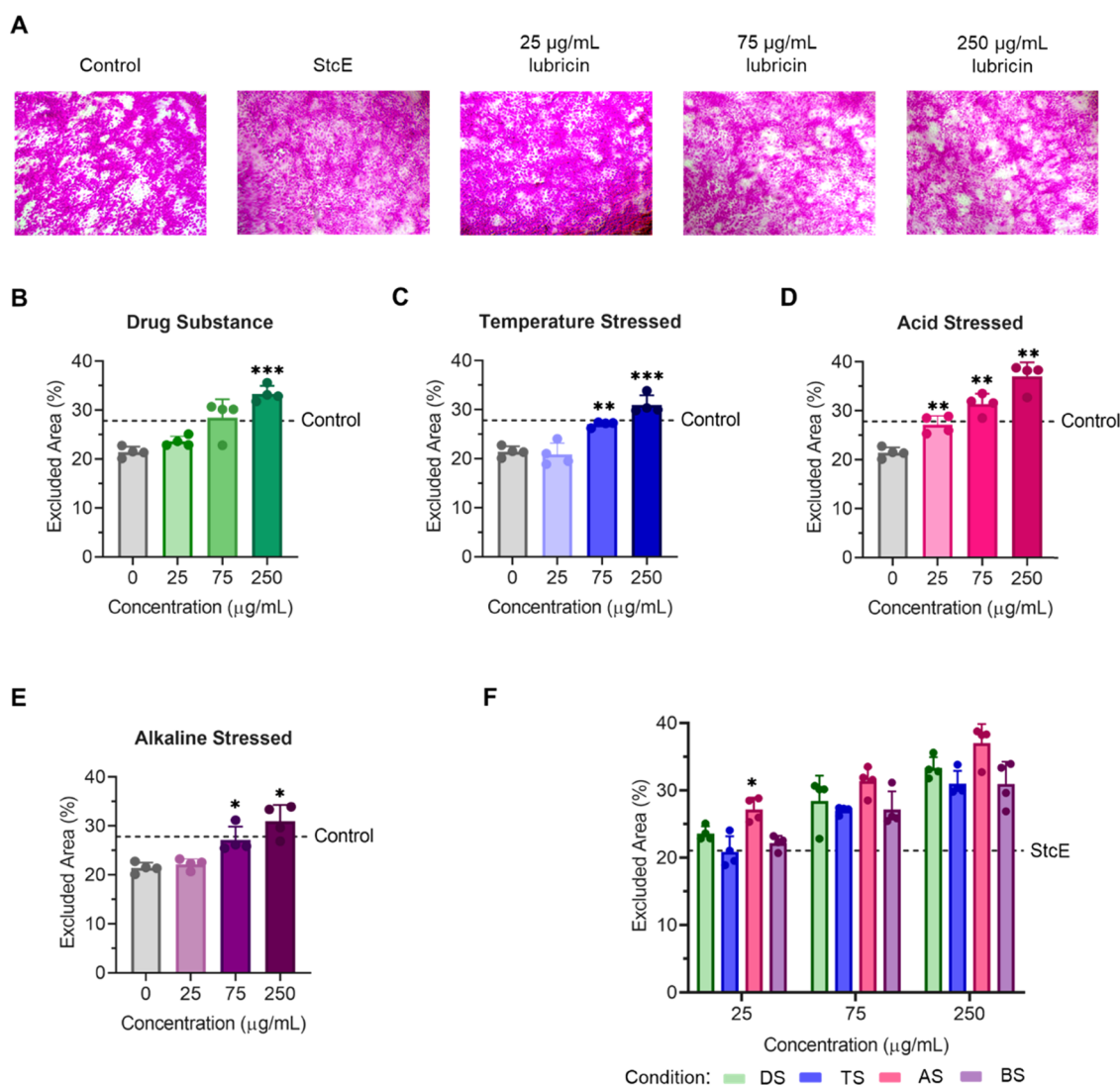


Figure 8. Lubricin supplementation reduced rose bengal penetrance in a dose-dependent manner for both unstressed and aged lubricin on differentiated hTCEpi cells. (A) StcE-induced mucin deficiency increased dye penetrance, which was attenuated by recombinant human lubricin in a dose-dependent manner. (B–E) Supplementation with higher concentrations of (B) lubricin or lubricin subjected to (C) temperature stress, (D) acid stress, or (E) alkaline stress resulted in an increased rose bengal-negative area. (F) Trends in the excluded area for different lubricin variants were consistent across three concentrations (25, 75, and 250 $\mu\text{g/mL}$). Statistical significance ($p < 0.05$) was determined using one-way Welch's ANOVA with post-hoc Dunnett's T3 multiple comparisons testing relative to StcE-treated (0 $\mu\text{g/mL}$) cells (B–E) or unstressed drug substance (DS) (F).

II.V. Lubricin Adsorption Depends on Both Concentration and Conformation. It has previously been reported that lubricin aggregates and multimers exhibit differential dose responses in cartilage-on-cartilage friction tests compared to monomers, suggesting different adsorption behavior.⁴⁸ To interrogate how lubricin conformation affects adsorption, StcE-treated hTCEpi and HCjE cells were incubated in a lubricin-supplemented cell culture medium for 2 h and then immunostained using an anti-PRG4 antibody specific to lubricin's mucin-like domain. For each lubricin variant, adsorption was quantified using average gray values at three concentrations (25, 75, and 250 $\mu\text{g/mL}$) (Figures S5 and S6).

On both StcE-treated hTCEpi and HCjE cells, surface density increased with increasing lubricin solution concentration for all variants (Figures S5 and S6A–H). Intriguingly, temperature-stressed and alkaline-stressed lubricin molecules adsorbed less readily and in a patchier manner than unstressed drug substance, while acid-stressed lubricin adsorbed in similar

amounts but more uniformly (Figures 7, S6I–N, and S7). Because previous reports indicate that weaker lubricin–substrate adhesions correlate with more uniform coverage and chain density,¹⁹ the observed trends for acid-stressed lubricin suggest that lubricin molecules lacking one or more terminal domains bind less specifically to hTCEpi and HCjE cell surfaces.

II.VI. Lubricin Surface Concentration Determines Barrier Functionality but Not Antiadhesion and Bio-lubrication Properties. To interrogate how lubricin surface concentration and conformation affect barrier functionality, we incubated StcE-treated hTCEpi cells in cell culture medium containing recombinant lubricin at 25, 75, and 250 $\mu\text{g/mL}$ for 2 h before measuring rose bengal uptake. In contrast to lubricin's nonmonotonic antiadhesion properties on mucin-deficient corneal epithelial cells, dye penetrance was reduced as solution concentration increased for each lubricin variant (Figure 8). The association between dye uptake and lubricin

concentration is perhaps unsurprising as the presence of an oligosaccharide lattice crosslinked by galectin-3 protects against rose bengal penetrance.^{40,41,56} Because galectin-3, a 35-kDa β -galactoside-binding lectin, binds lubricin O-glycans expected to be accessible on both fragments and aggregates,^{57,58} we anticipated that lubricin conformation would not play a dominant role in imparting barrier functionality. Consistent with this hypothesis, the rose bengal excluded area was strongly correlated with lubricin surface coverage independent of surface conformation, with a nonparametric Spearman correlation coefficient of 0.93 ($p < 0.0001$) (Figure S8A).

In contrast with lubricin-imparted barrier protection, lubricin's antiadhesion behavior on StcE-treated differentiated hTCEpi cells and biolubrication properties appeared to be more conformation dependent. Based on nonparametric Spearman correlation analysis, the correlations between surface coverage and its antiadhesion and biolubrication properties are weak (Figure S8B–D), indicating that lubricin surface concentration is not activity-determining. Instead, the glycoprotein's antiadhesion and biolubrication properties appear to be associated with its conformation. Specifically, more aggregated samples, particularly alkaline-stressed lubricin, behave differently than fragmented, acid-stressed lubricin molecules. As recombinant human lubricin aggregation and fragmentation can occur during manufacturing and storage, the conformation-dependent phenotypic responses observed on our dry eye mimetic ocular surfaces highlight the importance of employing physiological substrates in both the drug screening and mechanistic studies.

III. CONCLUSIONS

In this work, we present a comprehensive *in vitro* mucin-deficient ocular surface platform for drug screening that models the biophysical and biochemical properties of the corneal and conjunctival epithelium, as well as dysfunctions that emerge when ocular surface mucin presentation is altered. Illustratively, the Mu-DeMOS-based platform mimics DED symptomatology such as increased cell–cell adhesion, increased cell adhesion strength, and reduced barrier functionality. We exploit this imaging-friendly, cell-based platform to show that the investigational DED therapeutic lubricin can partially or fully reverse indicators of ocular surface dysfunction *in vitro*, with similar amounts of adsorbed lubricin exerting differential effects on adhesion prevention, biolubrication, and barrier functionality based on pretreatment incubation conditions. Together, these findings highlight lubricin's promise as a DED therapeutic and demonstrate that the Mu-DeMOS platform is a powerful tool for screening clinically relevant properties of ocular biolubricants.

IV. MATERIALS AND METHODS

IV.I. Materials. Reagents were purchased from either Sigma-Aldrich or Fisher Scientific and used without further purification, unless otherwise noted. Recombinant StcE enzyme was graciously donated by Kayvon Pedram and Prof. Carolyn Bertozzi (Stanford University).³⁶

IV.II. Recombinant Human Lubricin. Recombinant human lubricin was generously provided by Novartis (Basel, Switzerland) at a concentration of 2.01 mg/mL (including O-glycosylation) in 10 mM sodium phosphate, 140 mM sodium chloride, and 0.02% (w/v) polysorbate 20, pH 7.0. Acid-stressed lubricin was prepared by adjusting solution pH to 4.0 and incubating the solution for 2 weeks at 40 °C. Alkaline-stressed lubricin was prepared by adjusting solution

pH to 9.0 and incubating the solution for 2 weeks at 40 °C. Temperature-stressed lubricin was prepared by incubating the solution without pH adjustment for 4 weeks at 40 °C. Size-exclusion chromatography was used to evaluate lubricin aggregation and fragmentation following accelerated aging. Samples were stored at –80 °C and used without further purification.

IV.III. HCjE and hTCEpi Cell Culture. Human telomerase reverse transcriptase-immortalized conjunctival epithelial (HCjE) cells were obtained as a gift from Prof. Ilene Gipson (Schepens Eye Research Institute, Harvard Medical School) via the Wu Lab (Stanford University School of Medicine).²⁶ HCjE cells were used between passages 6 and 20. Human telomerase reverse transcriptase-immortalized corneal epithelial (hTCEpi) cells were graciously donated by Prof. Suzanne Fleiszig (University of California Berkeley).²⁷ hTCEpi cells were used between passages 55 and 70. Cells were cultured in growth medium composed of EpiLife medium with 60 μ M calcium (Gibco MEPI500CA) supplemented with 1% penicillin–streptomycin (Gibco 15140122) and Human Corneal Growth Supplement (HCGS) (Gibco S0095) on tissue culture-treated plastic.

IV.IV. Live Cell Rheometer. The basic design and implementation of the LCR have been previously described.^{29–31} Briefly, the instrument consists of a custom-built bottom plate on which corneal epithelial or conjunctival cells were cultured. This bottom plate was mounted on an inverted microscope (Nikon Eclipse Ti-S, Nikon), and cells were visualized using a 40 \times air objective (Nikon) at ambient temperature and humidity. The average temperature across the human ocular surface varies between 32.9 and 36 °C,⁵⁹ however, measurements were conducted under ambient conditions to improve reproducibility. Similar conditions were previously used for tissue-on-tissue and tissue-on-hydrogel friction measurements in the presence of lubricin.^{22,23,49} A custom-built top plate was carefully inverted over the cells cultured on the bottom plate and allowed to settle by gravity. The resulting normal stress permitted good contact between the stratified cell layers without inducing blebbing or cell lysis. The top plate consisted of a 12 mm circular glass coverslip attached to a 3D printed custom top plate, as described below. The outer surface of the glass coverslip with cultured cells was in contact with the stratified cell layers on the bottom plate. A force transducer attached to a piezoelectric stage was brought into contact with the custom stand on the top plate. Lateral motion of the piezoelectric stage and attached force transducer pushed the top plate along the stratified cells on the bottom plate, shearing the cells.

IV.V. Bottom Plate Preparation. A 35 mm glass-bottom cell culture dish (#1.5, 20 mm well, Cellvis D35201.SN) was coated with bovine collagen coating solution (Cell Applications Inc. 12550) for at least 30 min at 37 °C or overnight at 4 °C. Excess collagen solution was removed, and the coverslip was rinsed three times with PBS and dried in a tissue culture hood. To allow contact between the force transducer and the custom stand on the top plate during LCR measurements, one-quarter to one-third of the upper rim of the glass-bottom dish, measured in the circumferential direction, was manually removed under sterile conditions prior to collagen coating.

hTCEpi or HCjE cells were detached from their culture flask and suspended in growth medium, counted using a hemocytometer, adjusted to a density of \sim 250,000 cell/mL, and 500 μ L of the cell suspension was deposited into the well of the glass-bottom plate. After incubation for 2–3 h at 37 °C and 5% CO₂, which gave the cells time to attach to the glass bottom, 1.5 mL of growth medium was added to the bottom plate for further incubation. After the cells reached confluency, the growth medium was replaced by stratification medium (DMEM/F12 medium with high calcium (1 mM CaCl₂), 10% fetal bovine serum, and 10 ng/mL EGF). Cells were cultured in stratification medium for 6 or 7 days prior to LCR experiments; no substantial differences in cellular phenotype or mucin expression were observed between days 6 and 7. To induce mucin deficiency, the stratification medium was replaced by stratification medium containing 0.5 μ g/mL StcE the night before an experiment. The recombinant StcE enzyme was graciously donated by Prof. Carolyn Bertozzi (Stanford University).³⁶ Prior to the LCR experiment, the

cells were washed three times with Dulbecco's phosphate-buffered saline (DPBS) containing calcium and magnesium ions and 2 mL of the treatment medium was added. The treatment medium was composed of an 87.5% (v/v) CO₂ independent stratification medium supplemented with recombinant lubricin to the desired concentration. Phosphate-buffered saline (PBS) without calcium and magnesium was added to volume to maintain a constant background level of nonspecific protein interactions.

IV.VI. Top Plate Preparation. To prepare the custom-made top plate, a 12 mm glass coverslip was attached to a 3D printed custom plastic stand with 4 legs around a circular rim using a small amount of Norland Optical Adhesive 61 (NOA 61). The optical glue was cured by exposing the top plate to 365 nm UV light (UVLMS-38 EL Series 3-UV lamp, 8-W) for at least 30 min. To reduce interactions between the force transducer and the top plate stand, the circular rim was coated with a thin layer of NOA 61 and allowed to cure for 2–3 days under a 365 nm UV light source. The top plate was cleaned in Milli-Q water (~30 min, 2–3×) and isopropanol (~30 min) in an ultrasonic bath sonicator. After drying the top plates under a N₂ atmosphere, further cleaning was achieved using a Diener Pico Oxygen Plasma Cleaner (4–5 min).

The top side of the glass coverslip on the top plate was coated with bovine collagen coating solution for at least 30 min at 37 °C or overnight at 4 °C. HCjE cells were detached from their culture flask and suspended in growth medium, counted using a hemocytometer, adjusted to a density of ~350,000 cell/mL, and 200 μL of the cell suspension was deposited onto the top side of the glass coverslip. Cells were cultured on top plates in 24-well culture plates (one top plate per well). After incubation for 2–3 h at 37 °C and 5% CO₂, which gave the cells time to attach to the glass coverslip, 2 mL of growth medium was added to the well containing the top plate for further incubation. After the cells reached confluency, the growth medium was replaced by stratification medium (DMEM/F12 medium with high calcium (1 mM CaCl₂), 10% fetal bovine serum, and 10 ng/mL EGF). Cells were cultured in stratification medium for 6 or 7 days prior to LCR experiments; no substantial differences in cellular phenotype or mucin expression were observed between days 6 and 7. To induce mucin deficiency, the stratification medium was replaced by stratification medium containing 0.5 μg/mL StcE the night before an experiment. Prior to the LCR experiment, the cells were washed three times with DPBS containing calcium and magnesium ions and 2 mL of stratification medium was added to each well.

As the 3D printed custom plastic stand was reused in different experiments, cleaning of the stand was achieved by separating the glass coverslip from the stand and sonicating the stand in 10% (v/v) sodium dodecyl sulfate (~15 min) followed by Milli-Q water (~10 min, 2–3×).

IV.VII. Step-Strain Experiment. Following removal of the stratification medium, the top plate coated with stratified HCjE cells was slowly inverted over the bottom plate and allowed to settle by gravity. After a period of at least 2 h at 37 °C, the plates were placed on the inverted microscope under ambient conditions. The experiment was controlled by a customized MATLAB code. A force transducer attached to a piezoelectric stage was then gently brought into contact with the rim of the top plate, and a user-defined step motion was applied through the micromanipulator. To perform a step strain, the piezoelectric stage was programmed to push the top plate along the bottom plate ($l = 5 \mu\text{m}$) and hold the final position ($t = 2 \text{ min}$). A DAQ board (DAQ USB6008, National Instruments) collected the voltage readings as a function of time from the force sensor, which were converted to force levels, using a known conversion factor given by the manufacturer. During and after the top plate motion, a custom LabView code recorded the applied force (F) measured by the force transducer and a CCD camera (GuppyPro F-125 B, Allied Vision) connected to the microscope recorded the movement of the top plate and deformation of the cells. After the initial step-strain motion, the force was recorded for 2 min and then the force transducer was retracted and was no longer in contact with the top plate. After a waiting period of 2 min, allowing the system to re-equilibrate, the force transducer was again gently brought into

contact with the top plate and a second step-strain experiment was performed.

IV.VIII. Calculation of the Relaxation Modulus. To calculate the stress, σ , the force measured by the force transducer (F) was divided by the contact area between the stratified cell layers, which was assumed to be the area of the 12 mm glass coverslip ($A = 113 \text{ mm}^2$). Thus, the stress as a function of time was calculated by $\sigma(t) = \frac{F(t)}{A}$. The strain, γ , was calculated from the lateral displacement of the top plate (l) and the gap distance between the top and bottom plates (d), i.e., $\gamma = l/d$. The shear relaxation modulus was then calculated as $G(t) = \frac{\sigma(t)}{\gamma}$. Each trial was performed with new stratified cell layers and is presented as the average of two step-strain experiments conducted on the same pair of cells.

To estimate the gap distance between the top and bottom plates for LCR experiments, top and bottom plates were prepared as described above, washed 3× with DPBS containing calcium and magnesium ions, and incubated for 30 min at 37 °C, 5% CO₂ in DMEM/F12 with Hoechst (1:1000). Cells were then washed once with DPBS containing calcium and magnesium ions and 2 mL of treatment medium was added. The treatment medium was composed of the 87.5% (v/v) CO₂ independent stratification medium supplemented with recombinant lubricin to the desired concentration. PBS without calcium and magnesium was added to volume to maintain a constant background level of nonspecific protein interactions. Top and bottom plates were then brought into contact and allowed to adhere for at least 2 h at 37 °C as described above. Cells were imaged using a Nikon LSM780 confocal microscope. Images were analyzed using ImageJ software (NIH), with the gap distance estimated from the normalized fluorescent intensity averaged across the x - y plane as a function of z -axis height.

IV.IX. Rose Bengal Dye Penetration. Rose bengal was dissolved in PBS at a concentration of 0.1% (w/v) and sterile-filtered prior to use. Rose bengal uptake was determined using a modified literature protocol.⁶⁰ Briefly, cells were seeded in growth medium on 48-well tissue culture-treated plates treated with bovine collagen coating solution (Cell Applications Inc. 12550) at 37 °C and 5% CO₂ until they reached 100% confluence. After the cells reached confluency, the growth medium was replaced by stratification medium to induce differentiation and stratification. To induce mucin deficiency, the stratification medium was replaced by stratification medium containing 0.5 μg/mL StcE the night before an experiment. After 7 days under differentiation conditions, the cell culture medium was manually aspirated and the cells were rinsed three times with DPBS containing calcium and magnesium ions, followed by incubation with 400 μL of treatment medium. The treatment medium was composed of 87.5% (v/v) 1:1 DMEM/F12:growth medium supplemented with recombinant lubricin to the desired concentration. PBS without calcium and magnesium (or vehicle/formulation buffer (10 mM sodium phosphate, 140 mM sodium chloride, 0.02% (w/v) polysorbate 20, pH 7.0) where indicated) was added to volume to maintain a constant background level of nonspecific protein interactions. After 2 h incubation at 37 °C and 5% CO₂, the treatment medium was manually aspirated and washed three times with DPBS without calcium and magnesium ions, followed by incubation with rose bengal solution for 5 min at room temperature. The rose bengal solution was aspirated, and the cell layers were washed once with DPBS without calcium and magnesium. Cell layers were photographed in 3–4 locations per well using an inverted microscope (EVOS XL Core Imaging System).

Images were analyzed using ImageJ software (NIH), with the excluded area per well averaged for the 3–4 fields of view. To determine the excluded area in each image, the color balance was first corrected using the BIOP SimpleColorBalance plugin and then the pink stain was isolated using the Color Deconvolution plugin. Thresholding of the pink channel was used to quantify the rose bengal-negative area.

IV.X. Antiadhesion Measurements. Cells were seeded in growth medium on eight-well glass-bottom chamber slides treated

with bovine collagen coating solution (Cell Applications Inc. 12550) at 37 °C and 5% CO₂ until they reached 100% confluence. After the cells reached confluency, the growth medium was replaced by stratification medium to induce differentiation and stratification. To induce mucin deficiency, the stratification medium was replaced by stratification medium containing 0.5 μg/mL StcE the night before an experiment. After 7 days under differentiation conditions, the cell culture medium was manually aspirated and the cells were rinsed three times with DPBS containing calcium and magnesium ions, followed by incubation with 400 μL of treatment medium. The treatment medium was composed of the 87.5% (v/v) CO₂ independent stratification medium supplemented with recombinant lubricin to the desired concentration. PBS without calcium and magnesium (or vehicle/formulation buffer (10 mM sodium phosphate, 140 mM sodium chloride, 0.02% (w/v) polysorbate 20, pH 7.0) where indicated) was added to volume to maintain a constant background level of nonspecific protein interactions.

After 1.5 h incubation at 37 °C and 5% CO₂, the treatment medium was manually aspirated and cell suspension was added (400 μL/well). To prepare cell suspension, undifferentiated HCjE cells were trypsinized, resuspended in growth medium containing 1 μM CellTracker Deep Red (Invitrogen), and incubated at 37 °C and 5% CO₂ for 30 min. CellTracker Deep Red-stained HCjE cells were counted, centrifuged, and resuspended in adhesion medium at 50,000 cells/mL. The adhesion medium was composed of the 87.5% (v/v) 1:1 DMEM/F12:growth medium supplemented with recombinant lubricin to the desired concentration. PBS without calcium and magnesium (or vehicle/formulation buffer (10 mM sodium phosphate, 140 mM sodium chloride, 0.02% (w/v) polysorbate 20, pH 7.0) where indicated) was added to volume to maintain a constant background level of nonspecific protein interactions. Samples were washed twice with DPBS containing calcium and magnesium ions, fixed with 4% paraformaldehyde in DPBS containing calcium and magnesium ions, washed, and imaged. Maximum projection images (8 FOV per sample) were analyzed using ImageJ software (NIH). Adherent cell counts were normalized for each cell type based on adherent cell counts on control cell layers in the treatment and adhesion medium without lubricin.

IV.XI. Lubricin Immunofluorescence. Cells were seeded in growth medium on eight-well glass-bottom chamber slides treated with bovine collagen coating solution (Cell Applications Inc. 12550) at 37 °C and 5% CO₂ until they reached 100% confluence. After the cells reached confluency, the growth medium was replaced by stratification medium to induce differentiation and stratification. To induce mucin deficiency, the stratification medium was replaced by stratification medium containing 0.5 μg/mL StcE the night before an experiment. After 7 days under differentiation conditions, the cell culture medium was manually aspirated and the cells were rinsed three times with DPBS containing calcium and magnesium ions, followed by incubation with 400 μL of treatment medium. The treatment medium was composed of the 87.5% (v/v) CO₂ independent stratification medium supplemented with recombinant lubricin to the desired concentration. PBS without calcium and magnesium was added to volume to maintain a constant background level of nonspecific protein interactions. After 2 h incubation at 37 °C and 5% CO₂, the treatment medium was manually aspirated and fixed with 4% (w/v) paraformaldehyde in DPBS containing calcium and magnesium ions for 15 min at room temperature. Samples were then washed three times with DPBS without calcium and magnesium ions, blocked with 5% w/v BSA and 5% v/v goat serum in PBS, and treated with the mouse anti-PRG4 (EMD Millipore MABT401, 1:1000) antibody in 2.5% w/v BSA and 2.5% v/v goat serum in PBS overnight at 4 °C. The samples were washed and then stained with goat anti-mouse AF488 (1:500, Life Technologies). DAPI was included as a nuclear counterstain. Samples were imaged using a Nikon LSM780 confocal microscope with the same settings for all conditions for each cell type.

Images were analyzed using ImageJ software (NIH). Average gray values were measured for maximum projections using ImageJ, corrected by subtracting background fluorescence, and normalized

based on the mean corrected average gray values measured for 25 μg/mL unstressed recombinant human lubricin. Correction and normalization were performed independently for hTCEpi and HCjE cells. Background fluorescence was measured as the average gray value for control and StcE-treated cells not incubated with exogenous lubricin. No statistically significant difference in fluorescence was observed between control and StcE-treated cells (hTCEpi: $p = 0.29$; HCjE: $p = 0.61$). To generate pixel intensity histograms, maximum projections were saved as text images and binned in 10 pixel intensity units. Relative frequencies were calculated for each field of view and averaged (3 FOV per sample).

IV.XII. Statistical Analysis. Two-tailed Welch's t -tests were used for comparisons between two experimental groups. One-way analysis of variance (ANOVA) with Dunnett's T3 multiple comparisons testing was used for comparisons among more than two experimental groups. Nonparametric Spearman's correlation analysis was used to assess whether two variables varied together, with the Spearman's correlation coefficient r quantifying the direction and magnitude of correlation. p values of less than 0.05 were considered statistically significant (n.s. = not significant ($p > 0.05$), * $p < 0.05$, ** $p < 0.01$, *** $p < 0.001$, **** $p < 0.0001$). Independent biological replicates were used to determine n values. All statistical analyses were performed using GraphPad Prism 8 software.

■ ASSOCIATED CONTENT

Supporting Information

The Supporting Information is available free of charge at <https://pubs.acs.org/doi/10.1021/acsami.1c22280>.

Additional experimental procedures and data on mucin immunofluorescence imaging, gap distance measurements, and lubricin sample characterizations (PDF)

■ AUTHOR INFORMATION

Corresponding Author

David Myung – Department of Chemical Engineering, Stanford University, Stanford, California 94305, United States; Byers Eye Institute, Stanford University School of Medicine, Palo Alto, California 94303, United States; Email: david.myung@stanford.edu

Authors

Amy C. Madl – Department of Chemical Engineering, Stanford University, Stanford, California 94305, United States; orcid.org/0000-0003-1323-0385

Chunzi Liu – Department of Chemical Engineering, Stanford University, Stanford, California 94305, United States

Daniel Cirera-Salinas – Biologics Analytical Research and Development, Novartis Pharma AG, Basel 4002, Switzerland

Gerald G. Fuller – Department of Chemical Engineering, Stanford University, Stanford, California 94305, United States; orcid.org/0000-0002-2924-053X

Complete contact information is available at: <https://pubs.acs.org/doi/10.1021/acsami.1c22280>

Author Contributions

¹A.C.M. and C.L. contributed equally to this work. This study was designed by A.C.M. and C.L. The initial draft of the manuscript was written by A.C.M., which was edited by C.L., D.C.-S., D.M., and G.G.F. All authors have given approval for the final version of the manuscript.

Notes

The authors declare the following competing financial interest(s): Professor Fuller received a research grant from Novartis Pharma AG.

The data that support the findings of this study are available from the corresponding author upon reasonable request. No unexpected or unusually high safety hazards were encountered.

ACKNOWLEDGMENTS

The authors would like to thank Vipul Vachharajani for technical training and assistance on atomic force microscopy. This work was supported in part by a grant to the Fuller Lab from Novartis (Basel, Switzerland). Schematics presented throughout this manuscript were created using BioRender.com. Author D.M. was supported by the National Institutes of Health (National Eye Institute K08EY028176 and a Departmental P30-EY026877 core grant) as well as a core grant and Career Development Award from Research to Prevent Blindness (RPB).

REFERENCES

- (1) Baudouin, C.; Rolando, M.; Benitez Del Castillo, J. M.; Messmer, E. M.; Figueiredo, F. C.; Irkec, M.; Van Setten, G.; Labetoulle, M. Reconsidering the Central Role of Mucins in Dry Eye and Ocular Surface Diseases. *Prog. Retinal Eye Res.* **2019**, *71*, 68–87.
- (2) Gipson, I. K. Distribution of Mucins at the Ocular Surface. *Exp. Eye Res.* **2004**, *78*, 379–388.
- (3) Gipson, I. K.; Hori, Y.; Argüeso, P. Character of Ocular Surface Mucins and Their Alteration in Dry Eye Disease. *Ocul. Surf.* **2004**, *2*, 131–148.
- (4) Madl, A. C.; Fuller, G. F.; Myung, D. Modeling and Restoring the Tear Film. *Curr. Ophthalmol. Rep.* **2020**, *8*, 281–300.
- (5) Shimazaki, J. Definition and Diagnostic Criteria of Dry Eye Disease: Historical Overview and Future Directions. *Invest. Ophthalmol. Visual Sci.* **2018**, *59*, DES7–DES12.
- (6) Georgiev, G. A.; Eftimov, P.; Yokoi, N. Contribution of Mucins towards the Physical Properties of the Tear Film: A Modern Update. *Int. J. Mol. Sci.* **2019**, *20*, 6132.
- (7) Uchino, Y. The Ocular Surface Glycocalyx and Its Alteration in Dry Eye Disease: A Review. *Invest. Ophthalmol. Visual Sci.* **2018**, *59*, DES157–DES162.
- (8) Holland, E. J.; Darvish, M.; Nichols, K. K.; Jones, L.; Karpecki, P. M. Efficacy of Topical Ophthalmic Drugs in the Treatment of Dry Eye Disease: A Systematic Literature Review. *Ocul. Surf.* **2019**, *17*, 412–423.
- (9) Mantelli, F.; Argüeso, P. Functions of Ocular Surface Mucins in Health and Disease. *Curr. Opin. Allergy Clin. Immunol.* **2008**, *8*, 477–483.
- (10) Bansil, R.; Stanley, E.; Lamont, J. T. Mucin Biophysics. *Annu. Rev. Physiol.* **1995**, *57*, 635–657.
- (11) Danjo, Y.; Watanabe, H.; Tisdale, A. S.; George, M.; Tsumura, T.; Abelson, M. B.; Gipson, I. K. Alteration of Mucin in Human Conjunctival Epithelia in Dry Eye. *Invest. Ophthalmol. Visual Sci.* **1998**, *39*, 2602–2609.
- (12) McDonald, M.; Patel, D. A.; Keith, M. S.; Snedecor, S. J. Economic and Humanistic Burden of Dry Eye Disease in Europe, North America, and Asia: A Systematic Literature Review. *Ocul. Surf.* **2016**, *14*, 144–167.
- (13) Nebbioso, M.; Fameli, V.; Gharbiya, M.; Sacchetti, M.; Zicari, A. M.; Lambiase, A. Investigational Drugs in Dry Eye Disease. *Expert Opin. Invest. Drugs* **2016**, *25*, 1437–1446.
- (14) Lambiase, A.; Sullivan, B. D.; Schmidt, T. A.; Sullivan, D. A.; Jay, G. D.; Truitt, E. R.; Bruscolini, A.; Sacchetti, M.; Mantelli, F. A Two-Week, Randomized, Double-Masked Study to Evaluate Safety and Efficacy of Lubricin (150 Mg/ML) Eye Drops Versus Sodium Hyaluronate (HA) 0.18% Eye Drops (Vismed) in Patients with Moderate Dry Eye Disease. *Ocul. Surf.* **2017**, *15*, 77–87.
- (15) Coles, J. M.; Chang, D. P.; Zauscher, S. Molecular Mechanisms of Aqueous Boundary Lubrication by Mucinous Glycoproteins. *Curr. Opin. Colloid Interface Sci.* **2010**, *15*, 406–416.
- (16) Zappone, B.; Greene, G. W.; Oroudjev, E.; Jay, G. D.; Israelachvili, J. N. Molecular Aspects of Boundary Lubrication by Human Lubricin: Effect of Disulfide Bonds and Enzymatic Digestion. *Langmuir* **2008**, *24*, 1495–1508.
- (17) Zappone, B.; Ruths, M.; Greene, G. W.; Jay, G. D.; Israelachvili, J. N. Adsorption, Lubrication, and Wear of Lubricin on Model Surfaces: Polymer Brush-Like Behavior of a Glycoprotein. *Biophys. J.* **2007**, *92*, 1693–1708.
- (18) Greene, G. W.; Thapa, R.; Holt, S. A.; Wang, X.; Garvey, C. J.; Tabor, R. F. Structure and Property Changes in Self-Assembled Lubricin Layers Induced by Calcium Ion Interactions. *Langmuir* **2017**, *33*, 2559–2570.
- (19) Han, M.; Silva, S. M.; Lei, W.; Quigley, A.; Kapsa, R. M. I.; Moulton, S. E.; Greene, G. W. Adhesion and Self-Assembly of Lubricin (PRG4) Brush Layers on Different Substrate Surfaces. *Langmuir* **2019**, *35*, 15834–15848.
- (20) Lee, S.; Müller, M.; Rezwani, K.; Spencer, N. D. Porcine Gastric Mucin (PGM) at the Water/Poly(Dimethylsiloxane) (PDMS) Interface: Influence of pH and Ionic Strength on Its Conformation, Adsorption, and Aqueous Lubrication Properties. *Langmuir* **2005**, *21*, 8344–8353.
- (21) Das, S.; Banquy, X.; Zappone, B.; Greene, G. W.; Jay, G. D.; Israelachvili, J. N. Synergistic Interactions between Grafted Hyaluronic Acid and Lubricin Provide Enhanced Wear Protection and Lubrication. *Biomacromolecules* **2013**, *14*, 1669–1677.
- (22) Schmidt, T. A.; Sullivan, D. A.; Knop, E.; Richards, S. M.; Knop, N.; Liu, S.; Sahin, A.; Darabad, R. R.; Morrison, S.; Kam, W. R.; Sullivan, B. D. Transcription, Translation, and Function of Lubricin, a Boundary Lubricant, at the Ocular Surface. *JAMA Ophthalmol.* **2013**, *131*, 766–776.
- (23) Morrison, S.; Sullivan, D. A.; Sullivan, B. D.; Sheardown, H.; Schmidt, T. A. Dose-Dependent and Synergistic Effects of Proteoglycan 4 on Boundary Lubrication at a Human Cornea-Polydimethylsiloxane Biointerface. *Eye Contact Lens* **2012**, *38*, 27–35.
- (24) Fini, M. E.; Jeong, S.; Gong, H.; Martinez-Carrasco, R.; Laver, N. M. V.; Hijikata, M.; Keicho, N.; Argüeso, P. Membrane-Associated Mucins of the Ocular Surface: New Genes, New Protein Functions and New Biological Roles in Human and Mouse. *Prog. Retinal Eye Res.* **2020**, *75*, No. 100777.
- (25) Yáñez-Soto, B.; Leonard, B. C.; Raghunathan, V. K.; Abbott, N. L.; Murphy, C. J. Effect of Stratification on Surface Properties of Corneal Epithelial Cells. *Invest. Ophthalmol. Visual Sci.* **2015**, *56*, 8340–8348.
- (26) Gipson, I. K.; Spurr-Michaud, S.; Argüeso, P.; Tisdale, A.; Ng, T. F.; Russo, C. L. Mucin Gene Expression in Immortalized Human Corneal–Limbal and Conjunctival Epithelial Cell Lines. *Invest. Ophthalmol. Visual Sci.* **2003**, *44*, 2496–2506.
- (27) Robertson, D. M.; Li, L.; Fisher, S.; Pearce, V. P.; Shay, J. W.; Wright, W. E.; Cavanagh, H. D.; Jester, J. V. Characterization of Growth and Differentiation in a Telomerase-Immortalized Human Corneal Epithelial Cell Line. *Invest. Ophthalmol. Visual Sci.* **2005**, *46*, 470–478.
- (28) Shafai, S.; Hutter, V.; Cook, M. T.; Brown, M. B.; Chau, D. Y. S. *In Vitro* Cell Models for Ophthalmic Drug Development Applications. *BioRes. Open Access* **2016**, *5*, 94–108.
- (29) Liu, C.; Madl, A. C.; Cirera-Salinas, D.; Kress, W.; Straube, F.; Myung, D.; Fuller, G. G. Mucin-Like Glycoproteins Modulate Interfacial Properties of a Mimetic Ocular Epithelial Surface. *Adv. Sci.* **2021**, *8*, No. 2100841.
- (30) Ramos, T.; Scott, D.; Ahmad, S. An Update on Ocular Surface Epithelial Stem Cells: Cornea and Conjunctiva. *Stem Cells Int.* **2015**, *2015*, No. 601731.
- (31) Elkins, C. M.; Shen, W.-J.; Khor, V. K.; Kraemer, F. B.; Fuller, G. G. Quantification of Stromal Vascular Cell Mechanics with a Linear Cell Monolayer Rheometer. *J. Rheol.* **2015**, *59*, 33–50.
- (32) Elkins, C. M.; Qi, Q. M.; Fuller, G. G. Corneal Cell Adhesion to Contact Lens Hydrogel Materials Enhanced via Tear Film Protein Deposition. *PLoS One* **2014**, *9*, No. e105512.

- (33) Hollenbeck, E. C.; Antonoplis, A.; Chai, C.; Thongsomboon, W.; Fuller, G. G.; Cegelski, L. Phosphoethanolamine Cellulose Enhances Curli-Mediated Adhesion of Uropathogenic *Escherichia coli* to Bladder Epithelial Cells. *Proc. Natl. Acad. Sci. U.S.A.* **2018**, *115*, 10106–10111.
- (34) Inatomi, T.; Spurr-Michaud, S.; Tisdale, A. S.; Gipson, I. K. Human Corneal and Conjunctival Epithelia Express MUC1 Mucin. *Invest. Ophthalmol. Visual Sci.* **1995**, *36*, 1818–1827.
- (35) Sumiyoshi, M.; Ricciuto, J.; Tisdale, A.; Gipson, I. K.; Mantelli, F.; Argüeso, P. Antiadhesive Character of Mucin O-Glycans at the Apical Surface of Corneal Epithelial Cells. *Invest. Ophthalmol. Visual Sci.* **2008**, *49*, 197–203.
- (36) Malaker, S. A.; Pedram, K.; Ferracane, M. J.; Bensing, B. A.; Krishnan, V.; Pett, C.; Yu, J.; Woods, E. C.; Kramer, J. R.; Westerlind, U.; Dorigo, O.; Bertozzi, C. R. The Mucin-Selective Protease StcE Enables Molecular and Functional Analysis of Human Cancer-Associated Mucins. *Proc. Natl. Acad. Sci. U.S.A.* **2019**, *116*, 7278–7287.
- (37) Yu, A. C. Y.; Worrall, L. J.; Strynadka, N. C. J. Structural Insight into the Bacterial Mucinase StcE Essential to Adhesion and Immune Evasion during Enterohemorrhagic *E. coli* Infection. *Structure* **2012**, *20*, 707–717.
- (38) Grys, T. E.; Walters, L. L.; Welch, R. A. Characterization of the StcE Protease Activity of *Escherichia coli* O157:H7. *J. Bacteriol.* **2006**, *188*, 4646–4653.
- (39) Liu, C.; Pokki, J.; Scales, C. W.; Fuller, G. G. Tuning Corneal Epithelial Cell Adhesive Strength with Varying Crosslinker Content in Silicone Hydrogel Materials. *Transl. Vis. Sci. Technol.* **2020**, *9*, 3.
- (40) Gipson, I. K.; Spurr-Michaud, S.; Tisdale, A.; Menon, B. B. Comparison of the Transmembrane Mucins MUC1 and MUC16 in Epithelial Barrier Function. *PLoS One* **2014**, *9*, No. e100393.
- (41) Argüeso, P.; Tisdale, A.; Spurr-Michaud, S.; Sumiyoshi, M.; Gipson, I. K. Mucin Characteristics of Human Corneal-Limbal Epithelial Cells That Exclude the Rose Bengal Anionic Dye. *Invest. Ophthalmol. Visual Sci.* **2006**, *47*, 113–119.
- (42) Blalock, T. D.; Spurr-Michaud, S. J.; Tisdale, A. S.; Heimer, S. R.; Gilmore, M. S.; Ramesh, V.; Gipson, I. K. Functions of MUC16 in Corneal Epithelial Cells. *Invest. Ophthalmol. Visual Sci.* **2007**, *48*, 4509–4518.
- (43) Elsaid, K. A.; Jay, G. D.; Warman, M. L.; Rhee, D. K.; Chichester, C. O. Association of Articular Cartilage Degradation and Loss of Boundary-Lubricating Ability of Synovial Fluid Following Injury and Inflammatory Arthritis. *Arthritis Rheum.* **2005**, *52*, 1746–1755.
- (44) Chang, D. P.; Abu-Lail, N. I.; Guilak, F.; Jay, G. D.; Zauscher, S. Conformational Mechanics, Adsorption, and Normal Force Interactions of Lubricin and Hyaluronic Acid on Model Surfaces. *Langmuir* **2008**, *24*, 1183–1193.
- (45) Chang, D. P.; Abu-Lail, N. I.; Coles, J. M.; Guilak, F.; Jay, G. D.; Zauscher, S. Friction Force Microscopy of Lubricin and Hyaluronic Acid between Hydrophobic and Hydrophilic Surfaces. *Soft Matter* **2009**, *5*, 3438–3445.
- (46) Gleghorn, J. Boundary Mode Frictional Properties of Articular Cartilage: Functional Implications of Lubricin Localization, PhD Thesis, 2007 (<http://citeseerx.ist.psu.edu/viewdoc/download?doi=10.1.1.1009.9390&rep=rep1&type=pdf>).
- (47) Korogiannaki, M.; Samsom, M.; Schmidt, T. A.; Sheardown, H. Surface-Functionalized Model Contact Lenses with a Bioinspired Proteoglycan 4 (PRG4)-Grafted Layer. *ACS Appl. Mater. Interfaces* **2018**, *10*, 30125–30136.
- (48) Abubacker, S.; Ponjevic, D.; Ham, H. O.; Messersmith, P. B.; Matyas, J. R.; Schmidt, T. A. Effect of Disulfide Bonding and Multimerisation on Proteoglycan 4's Cartilage Boundary Lubricating Ability and Adsorption. *Connect. Tissue Res.* **2016**, *57*, 113–123.
- (49) Seo, J.; Byun, W. Y.; Alisafaei, F.; Georgescu, A.; Yi, Y.-S.; Massaro-Giordano, M.; Shenoy, V. B.; Lee, V.; Bunya, V. Y.; Huh, D. Multiscale Reverse Engineering of the Human Ocular Surface. *Nat. Med.* **2019**, *25*, 1310–1318.
- (50) Rhee, D. K.; Marcelino, J.; Baker, M.; Gong, Y.; Smits, P.; Lefebvre, V.; Jay, G. D.; Stewart, M.; Wang, H.; Warman, M. L.; Carpten, J. D. The Secreted Glycoprotein Lubricin Protects Cartilage Surfaces and Inhibits Synovial Cell Overgrowth. *J. Clin. Invest.* **2005**, *115*, 622–631.
- (51) Gleghorn, J. P.; Jones, A. R. C.; Flannery, C. R.; Bonassar, L. J. Boundary Mode Frictional Properties of Engineered Cartilaginous Tissues. *Eur. Cells Mater.* **2007**, *14*, 20–29.
- (52) Majd, S. E.; Kuijter, R.; Köwitsch, A.; Groth, T.; Schmidt, T. A.; Sharma, P. K. Both Hyaluronan and Collagen Type II Keep Proteoglycan 4 (Lubricin) at the Cartilage Surface in a Condition That Provides Low Friction during Boundary Lubrication. *Langmuir* **2014**, *30*, 14566–14572.
- (53) Gleghorn, J. P.; Jones, A. R. C.; Flannery, C. R.; Bonassar, L. J. Boundary Mode Lubrication of Articular Cartilage by Recombinant Human Lubricin. *J. Orthop. Res.* **2009**, *27*, 771–777.
- (54) Jones, A. R. C.; Gleghorn, J. P.; Hughes, C. E.; Fitz, L. J.; Zollner, R.; Wainwright, S. D.; Cateson, B.; Morris, E. A.; Bonassar, L. J.; Flannery, C. R. Binding and Localization of Recombinant Lubricin to Articular Cartilage Surfaces. *J. Orthop. Res.* **2007**, *25*, 283–292.
- (55) Swann, D. A.; Hendren, R. B.; Radin, E. L.; Sotman, S. L. The Lubricating Activity of Synovial Fluid Glycoproteins. *Arthritis Rheum.* **1981**, *24*, 22–30.
- (56) Mauris, J.; Mantelli, F.; Woodward, A. M.; Cao, Z.; Bertozzi, C. R.; Panjwani, N.; Godula, K.; Argüeso, P. Modulation of Ocular Surface Glycocalyx Barrier Function by a Galectin-3 N-Terminal Deletion Mutant and Membrane-Anchored Synthetic Glycopolymers. *PLoS One* **2013**, *8*, No. e72304.
- (57) Flowers, S. A.; Thomsson, K. A.; Ali, L.; Huang, S.; Mthembu, Y.; Regmi, S. C.; Holgersson, J.; Schmidt, T. A.; Rolfson, O.; Björkman, L. I.; Sundqvist, M.; Karlsson, A.; Jay, G. D.; Eisler, T.; Krawetz, R.; Karlsson, N. G. Core-2 O-Glycans Are Required for Galectin-3 Interaction with the Osteoarthritis Related Protein Lubricin. *bioRxiv* **2019**, No. 2019.12.20.884148.
- (58) Reesink, H. L.; Bonnevie, E. D.; Liu, S.; Shurer, C. R.; Hollander, M. J.; Bonassar, L. J.; Nixon, A. J. Galectin-3 Binds to Lubricin and Reinforces the Lubricating Boundary Layer of Articular Cartilage. *Sci. Rep.* **2016**, *6*, No. 25463.
- (59) Purslow, C.; Wolffsohn, J. S. Ocular Surface Temperature: A Review. *Eye Contact Lens Sci. Clin. Pract.* **2005**, *31*, 117–123.
- (60) Argüeso, P.; Gipson, I. K. Assessing Mucin Expression and Function in Human Ocular Surface Epithelia In Vivo and In Vitro. In *Mucins: Methods and Protocols*; McGuckin, M. A.; Thornton, D. J., Eds.; Methods in Molecular Biology; Humana Press: Totowa, NJ, 2012; pp 313–325.